BRAIN COMMUNICATIONS

KCNQ variants and pain modulation: a missense variant in Kv7.3 contributes to pain resilience

Jun-Hui Yuan,[1,2,3,*] Mark Estacion,[1,2,3,*] Malgorzata A. Mis,[1,2,3,*] Brian S. Tanaka,[1,2,3,*] Betsy R. Schulman,[1,2,3] Lubin Chen,[1,2,3] Shujun Liu,[1,2,3] Fadia B. Dib-Hajj,[1,2,3] Sulayman D. Dib-Hajj[1,2,3] and Stephen G. Waxman[1,2,3]

* These authors contributed equally to this work.

There is a pressing need for understanding of factors that confer resilience to pain. Gain-of-function mutations in sodium channel Nav1.7 produce hyperexcitability of dorsal root ganglion neurons underlying inherited erythromelalgia, a human genetic model of neuropathic pain. While most individuals with erythromelalgia experience excruciating pain, occasional outliers report more moderate pain. These differences in pain profiles in blood-related erythromelalgia subjects carrying the same pain-causative Nav1.7 mutation and markedly different pain experience provide a unique opportunity to investigate potential genetic factors that contribute to inter-individual variability in pain. We studied a patient with inherited erythromelalgia and a Nav1.7 mutation (c.4345T>G, p. F1449V) with severe pain as is characteristic of most inherited erythromelalgia patients, and her mother who carries the same Nav1.7 mutation with a milder pain phenotype. Detailed six-week daily pain diaries of pain episodes confirmed their distinct pain profiles. Electrophysiological studies on subject-specific induced pluripotent stem cell-derived sensory neurons from each of these patients showed that the excitability of these cells paralleled their pain phenotype. Whole-exome sequencing identified a missense variant (c.2263C>T, p. D755N) in *KCNQ3* (Kv7.3) in the pain resilient mother. Voltage-clamp recordings showed that co-expression of Kv7.2-wild type (WT)/Kv7.3-D755N channels produced larger M-currents than that of Kv7.2-WT/Kv7.3-WT. The difference in excitability of the patient-specific induced pluripotent stem cell-derived sensory neurons was mimicked by modulating M-current levels using the dynamic clamp and a model of the mutant Kv7.2-WT/Kv7.3-D755N channels. These results show that a 'pain-in-a-dish' model can be used to explicate genetic contributors to pain, and confirm that *KCNQ* variants can confer pain resilience via an effect on peripheral sensory neurons.

1 Department of Neurology, Yale University School of Medicine, New Haven, CT 06520, USA
2 Center for Neuroscience and Regeneration Research, Yale University School of Medicine, New Haven, CT 06520, USA
3 Center for Rehabilitation Research, VA Connecticut Healthcare System, West Haven, CT 06516, USA

Correspondence to: Stephen G. Waxman, MD, PhD
Neuroscience and Regeneration Research Center, VA Connecticut Healthcare System
950 Campbell Avenue, Building 34, West Haven, CT 06516, USA
E-mail: stephen.waxman@yale.edu

Keywords: Erythromelalgia; induced pluripotent stem cells; pain; potassium channel; whole-exome sequencing

Abbreviations: AP = action potential; BFNS = benign familial neonatal seizures; DRG = dorsal root ganglion; G–V = conductance–voltage; HEK293 = Human Embryonic Kidney Cells 293; IEM = inherited erythromelalgia; iPSC = induced pluripotent stem cell; I–V = current–voltage; MIMMendelian Inheritance in Man; NIS = neuronal imaging saline; NRS = numerical rating scale; PBS-T = phosphate buffered saline-tween; PFA = paraformaldehyde; RMP = resting membrane potential; SEM = mean ± standard error; WES = whole-exome sequencing; WT = wild type

Received July 13, 2021. Revised July 13, 2021. Accepted July 29, 2021. Advance Access publication September 8, 2021

Graphical Abstract

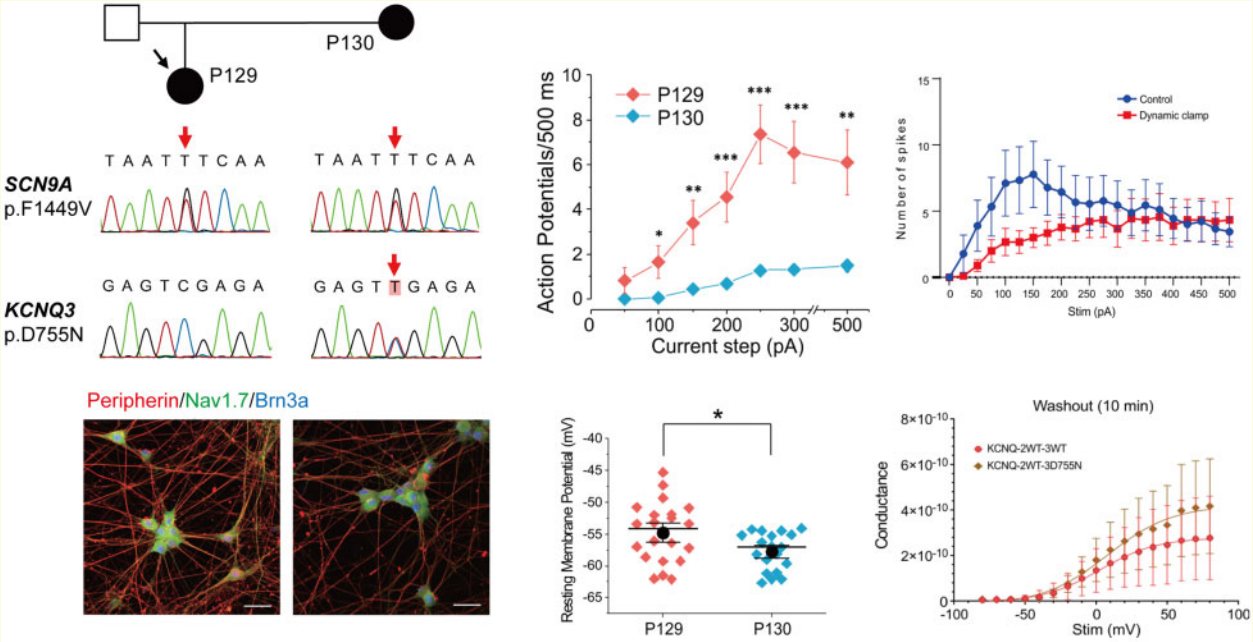

Introduction

There has been rapid progress in unravelling the genetics and genomics of pain in animal and human studies.[1–4] However, molecular factors that confer inter-individual variability in pain experience are not well understood and could result from a combination of factors, in the form of single nucleotide polymorphisms, epigenetic, environmental and social factors. While not underestimating the roles of epigenetic, psychological and environmental factors, initial studies in first-degree relatives of subjects with monogenic pain disorders with severe versus mild symptoms have shown that families with phenotypically discordant individuals provide a genetic substrate to identify gene variants that contribute to inter-individual differences in pain.[5]

Inherited erythromelalgia {IEM [Mendelian Inheritance in Man (MIM): 133020]} is an autosomal-dominant chronic pain disorder, in which pain is typically severe and caused by gain-of-function mutations in voltage-gated sodium channel Nav1.7 [encoded by *SCN9A* gene (MIM: 603415)],[6–8] which produce hyperexcitability of dorsal root ganglion (DRG) neurons,[9–11] thus providing a human model of neuropathic pain with a well-defined molecular basis. Pain in IEM is usually excrutiating. However, occasional outlier IEM patients, within the same family where most patients experience severe pain, display a much milder pain phenotype. While environmental, psychological and social factors contributing both resilience and vulnerability factors to pain,[12] pain resilience may also be influenced by genetic factors, as seen, for example, from the studies on gene variants associated with psychiatric disorders, like posttraumatic stress disorder and depression.[13–15]

We have used patient-specific induced pluripotent stem cells (iPSCs) and whole-exome sequencing (WES) to identify genetic factors that contribute to pain resilience. Previously, we studied a family with IEM in which pain characteristics of two subjects (mother/son) carrying the Nav1.7 mutation p. S241T were documented over a 6-week period and showed that total time in pain, number and duration of pain attacks and number of sleep awakenings due to pain, are markedly different between the two subjects.[16] This individual-to-individual variability in pain among members of a family carrying the same disease-causing mutation suggested the presence of private modulatory variants/mutations. We established patient-specific iPSC-derived sensory neuron (iPSC-SN),[17,18] and showed that the excitability of these neurons paralleled the pain phenotypes of the subjects suggesting the presence of a peripheral component to pain resilience. Using WES, we identified a rare gain-of-function variant in *KCNQ2* (MIM: 602235), the gene which encodes the voltage-gated potassium channel Kv7.2, in the pain resilient subject, and showed that this channel variant regulates the excitability of the iPSC-SN of this subject.[5]

Building on these earlier findings, here we study two individuals with different pain profiles from another family carrying a different Nav1.7 mutation (p.F1449V): a pair of daughter–mother with IEM (P129 and P130), at opposite ends of the pain spectrum, from a previously described pedigree.[10] We examined whether their

differences in pain might be paralleled by differences in firing properties of their peripheral sensory neurons, and further, asked whether we could identify any molecular contributors to the differences in neuronal excitability and pain profiles.

Materials and methods

Study design

A daughter (P129) and mother (P130) with documented gain-of-function mutation of Nav1.7-F1449V were invited to participate in this study. This clinical phenotyping study was conducted over a 6-week period where both subjects completed a daily pain diary in which the number and duration of attacks, severity of pain attacks and overall pain during the day, ongoing pain between attacks (if any), incidences of night awakening, duration of awakenings and triggers for pain were recorded. The subjects also recorded if they did not experience pain attacks on any given day. For ease of use, pain intensity was self-reported using the numerical rating scale (NRS) as the primary outcome, where 0 indicates no pain and 10 indicates the worst pain possible. The study was approved by the Human Investigation Committees at Yale University and the Veterans Affairs Medical Center, West Haven.

WES and data analysis

Whole blood samples were collected from the daughter and mother patients, and genomic DNA was extracted using the NucleoSpin Tissue kit (Machery-Nagel, Duren, Germany). Exome library preparation and sequencing were performed by the Yale Center for Genome Analysis as previously described.[5,19,20] Briefly, 1 µg of genomic DNA was applied to capture exome library using IDT xGen Exome Research Panel V1.0 (Integrated DNA Technologies, Coralville, IA, USA), and sequenced on the Illumina NovaSeq6000 platform using 101 bp paired-end sequencing reads according to Illumina protocols (Illumina Inc., San Diego, CA, USA). The obtained reads were aligned to the human genome reference (UCSC Genome Browser, hg19) using the BWA-MEM aligner. Genome Analysis Toolkit was utilized to create the variant call format files of variant calls.

The variant call format files were then processed for annotation and filtering using Ensembl Variant Effect Predictor (VEP) (v97.2) tool and in-house R scripts. Variants with coverage depth less than 10-fold or alteration frequency lower than 30% were removed. All variants were checked against the databases of 1000 Genomes, gnomAD, NHLBI-Go Exome Sequencing Project (ESP), UK10K and Yale whole-exome databases. Three in-silico tools were utilized to predict the pathogenicity, consisting of SIFT, PolyPhen-2 and CADD_phred (Combined Annotation Dependent Depletion), using the dbNSFP v3,0 plugin.[21] Ingenuity pathway analysis (IPA; version 43605602, QIAGEN) was used to carry out gene ontology analyses.

Generation of iPSCs and differentiation into sensory neurons

iPSCs were generated from the blood samples of P129 and P130, using CytoTune-iPS 2.0 Sendai Reprogramming Kit (Thermo Fisher Scientific) by the Yale Stem Cell Center according to the manufacturer protocol. Cells were screened for pluripotent stem cell markers and tested for normal karyotype before differentiation. iPSCs were cultured for at least 16 generations before the start of differentiation into sensory neurons. iPSCs were maintained and passaged using mTeSR plus medium (05827, StemCell Technologies, Canada). Differentiation into sensory neurons was previously described,[5] and followed a modified Chambers protocol with LSB and 3i inhibitors.[18,22] Differentiated neurons were maturated in Neurobasal Medium supplemented with N2/B27 GlutaMAX (Thermo Fisher Scientific) and four nerve growth factors [recombinant human β-nerve growth factor, brain-derived neurotrophic factor, glial-derived neurotrophic factor and neurotrophin-3 (25 ng/ml; PeproTech)] for more than 7 weeks before functional assessments.

PCR, reverse transcription PCR and Sanger sequencing

RNA was isolated from iPSC-SNs of P129 and P130 using the RNeasy Plus Kit (catalog #74134, Qiagen) according to the manufacturer's protocol. RNA concentration was measured on Nanodrop, and total RNA (100 ng) was used to generate cDNA using the iScript Reverse Transcription Supermix (Bio-Rad Laboratories, CA). One microliter of cDNA was used as a template for PCR amplification in a final volume of 25 µl.

Genomic DNA or cDNA were amplified using High Fidelity AccuPrime Taq DNA Polymerase according to the manufacturer's protocol (Cat#12346-086, Thermo Fisher Scientific). The following primers were used for Nav1.7-F1449V mutation for genomic DNA (5′-AAA CCTCAACAATGCTATGGC-3′ and 5′-AATCATAAG TTAGCCAGAACC-3′) and for cDNA (5′-TTAAGGG ATGGACGATTATTATGTATG-3′ and 5′-AGTGAAGTA GTAGTGTCTGAGGG-3′). Primers (5′-AGAGAAGAAGG AGGACAACAGG-3′ and 5′-AGATGCTGAAGCCACTT GGAG-3′) were designed for amplification of the fragment encompassing Kv7.3-D755N in both DNA and cDNA. Thermal cycling was initiated at 94°C for 2 min followed by 35 cycles of 15 s at 94°C, annealing for 30 s at 55°C, and an extension for 60 s at 68°C. PCR amplicons were sequenced at the Keck DNA Sequencing facility at Yale University.

Immunocytochemistry

Immunostaining for sensory neuron markers followed our previously described protocol.[5] Briefly, iPSC-SNs were fixed for 10 min with 4% paraformaldehyde (PFA) [20% PFA aqueous solution (Electron Microscopy Sciences, Hatfield, PA)] diluted in neuronal imaging saline (NIS). Primary antibodies, consisting of peripherin (chicken polyclonal, PER, Aves Labs; 1:2000), brn3a (mouse monoclonal, MAB1585, MilliporeSigma; 1:200), Nav1.7 (rabbit polyclonal, Y083; 1:250) were incubated overnight at 4°C in phosphate buffered saline-tween (PBS-T) (0.1% Triton X-100, 2% BSA, 4% donkey serum in PBS). Secondary antibodies, including donkey anti-chicken Alexa Fluor 488 (Jackson Immunoresearch, AB2340375; 1:1000), donkey anti-rabbit Alexa Fluor 594 (Life Technologies, A21207; 1:1000) and donkey anti-mouse Alexa Fluor 647 (Jackson Immunoresearch, 715-605-150; 1:1000), were incubated for 2 h at room temperature in PBS-T. Images were acquired using a two-photon confocal laser scanning microscope (Nikon A1R HD).

Whole-cell current-clamp electrophysiology of iPSC-SNs

Whole-cell current-clamp experiments were performed using an Axon MultiClamp 700B and an analogue to digital converter Digidata 1440a, as described previously.[5] Briefly, the data were filtered at 5 kHz, acquired at 50 kHz, and stored on a computer using the pClamp 10.6 software. Electrodes used for the recordings had resistance of <1.5 MΩ when filled with the internal solution, which consisted of (mM): KCl 140; HEPES, 5; EGTA, 0.5; Mg-ATP, 3; Dextrose 20; pH 7.3, 295–300 mOsm. The external recording solution contained (mM): NaCl, 140; KCl, 3; HEPES-NaOH, 10; $MgCl_2$, 2; $CaCl_2$, 2; Dextrose, 15; pH 7.3, ~320 mOsm.

iPSC-SNs with stable membrane potential were chosen for analysis. Resting membrane potential (RMP) was determined immediately after switching into current-clamp mode. Current threshold was defined as the minimum amount of current necessary to trigger an action potential (AP). The firing rate was determined by quantifying the number of APs generated in response to incremental depolarizing 500 ms current steps.

Transfection of Human Embryonic Kidney Cells 293 cells and whole-cell voltage-clamp recordings

Sequence encoding fluorescent protein, mRuby or mCitrine, was cloned upstream of the Kv7.2-WT or Kv7.3-WT ATG start site, respectively, with a 'stopGo' 33 amino acid 2A linker to permit fluorescent protein and Kv7 channel expression independently from the same mRNA transcript, as previously described.[23,24] The Kv7.3-D755N mutation was introduced into the Kv7.3-WT construct using QuickChange XL site-directed mutagenesis kit (Stratagene, La Jolla, CA). Human Embryonic Kidney Cells 293 (HEK293) cells, grown under standard culture conditions (5% CO_2, 37°C) in Dulbecco's modified Eagle's medium supplemented with 10% foetal bovine serum, were transiently transfected with the Kv7.2 and Kv7.3 alpha subunits using LipoJet (SignaGen laboratories, Frederick, MD). The transfected cells were resuspended and plated onto coverslips the next day and then patch-clamp recordings were performed over the next two days.

Whole-cell voltage-clamp recordings were performed on isolated HEK293 cells showing mRuby and mCitrine fluorescence at room temperature (~21°C). Electrodes were pulled from 1.65 mm O.D. borosilicate glass micropipettes (World Precision Instruments, Sarasota, FL) and had a resistance of 1–2 MΩ when filled with pipette solution, which contained (in mM): 126 K-Gluconate, 4 KCl, 10 HEPES, 0.3 EGTA, 10 phosphocreatinine disodium salt, 4 ATP Mg-salt and 0.3 GTP Na-salt (pH 7.3 with KOH, adjusted to 320 mOsm with dextrose). The extracellular solution contained (in mM): 140 NaCl, 3 KCl, 1 $MgCl_2$, 1 $CaCl_2$, 10 HEPES (pH 7.3 with NaOH, adjusted to 320 mOsm with dextrose). Currents of Kv7 channels were measured on an EPC-10 USB amplifier (HEKA Electronics) and acquired using PatchMaster software (HEKA Electronics) at an acquisition rate of 20 kHz with a low pass Bessel filter setting of 5 kHz. When appropriate, linear leak currents and capacitance artefacts were subtracted out using the P/N method.

To evaluate the voltage-dependence of Kv7 current, the activation protocol was performed as follows: from a holding potential of −80 mV, incrementing depolarizing pulses of 500 ms duration were stepped starting at −80 mV to +80 mV in 10 mV increments followed by a fixed hyperpolarizing pulse to −120 mV for 50 ms and then returning to holding potential. The pulse protocol was performed with P/4 leak subtraction and the sweep to sweep cycle time is 5 s. The current–voltage (I–V) relationship was computed as the average current measured during the last 50 ms of the depolarizing pulse. The large amplitude of the currents would be expected to result in progressively larger voltage-errors with large depolarizing stimuli due to incomplete series resistance compensation, and these would be expected to distort the I–V relation and complicate transformation of the I–V into a conductance–voltage (G–V) curve. Because of this, series resistance compensation was enabled and 90% compensation was commonly achieved. The G–V relationship was determined by measuring the instantaneous inward current during the repolarizing pulse to a fixed potential of −120 mV, which produces smaller currents due to the reduced driving force for potassium and results in smaller series resistance induced voltage errors. The instantaneous inward current recorded in this way reflect the total

number of channels opened by the preceding depolarizing pulse and result in a G–V curve that does not require determining the apparent reversal potential. The activation protocol was repeated multiple times after initiating whole-cell configuration to evaluate possible time-dependent changes in activation properties.

Whole-cell current-clamp and dynamic-clamp analyses of iPSC-SNs

Whole-cell current-clamp and dynamic-clamp experiments were performed using a HEKA EPC-800 amplifier connected to both an analogue to digital converter Digidata 1440a as well as Power 1401 interface from Cambridge Electronic Design to implement dynamic-clamp as described previously.[5] Briefly, the data were filtered at 5 kHz, acquired at 50 kHz, and stored on a computer using pClamp 10.6 software. Electrodes used for the recordings had resistance of <2 MΩ when filled with the internal solution, which consisted of (mM): 126 K-Gluconate, 4 KCl, 10 HEPES, 0.3 EGTA, 10 phosphocreatinine disodium salt, 4 ATP Mg-salt and 0.3 GTP Na-salt (pH 7.3 with KOH, adjusted to 320 mOsm with dextrose). The external recording solution contained (mM): NaCl, 140; KCl, 3; HEPES-NaOH, 10; $MgCl_2$, 2; $CaCl_2$, 2; Dextrose, 15; pH 7.3, ~320 mOsm.

iPSC-SNs with stable membrane potential were chosen for analysis. RMP was determined immediately after switching into current-clamp mode. To perform dynamic-clamp experiments, the firing rate was determined by quantifying the number of APs generated in response to incremental depolarizing 1000 ms current steps with the KCNQ conductance either OFF or ON with a target level of conductance corresponding to the average difference in current between Kv7.3-D755N and Kv7.3-WT. Because each cell is its own control, the averaged data were analysed with ANOVA of repeated measures.

Statistical analysis

Recorded electrophysiological data were processed offline using pClamp v10.6 (Molecular Devices, Sunnyvale, CA), Origin 2017/2018 (OriginLab Corporation, Northhampton, MA) and Excel (Microsoft, Redmond, WA). Data were analysed using Fitmaster (HEKA Electronics), SPSS24 (SPSS Inc., Chicago, IL), Origin and GraphPad Prism (GraphPad Software, San Diego, CA). Unless otherwise stated, data were expressed as mean ± standard error (SEM). Statistical tests used for each individual data set and *P*-values are stated in the Results section.

Data availability

All information necessary to evaluate the findings of the paper are included in the paper. Additional data can be provided from the authors upon request.

Results

Different pain profiles in two subjects carrying the same Nav1.7 mutation (p.F1449V)

Both subjects carry the p. F1449V mutation in the *SCN9A* gene that encodes Nav1.7. Both the daughter (P129) and mother (P130) patients describe the onset of pain attacks early in childhood. However, they were chosen for study because of differences in their pain profiles, as reflected in their histories (this paragraph) and in pain diaries (next paragraph). As is typical for patients with inherited erythromelalgia, both subjects reported that attacks were triggered by warm temperature, walking or exercise. The P129 daughter, 53-year-old at the time of study, reported a life-long history of frequent episodes of excruciating pain in the hands and feet, similar to multiple other members of her family who carry the p. F1449V mutation. The P130 mother, 81-year-old at the time of study, had a much milder pain profile than other family members who carried the p. F1449V mutation, and reported only very mild pain episodes that were much less frequent and much less severe. The P130 mother consistently reported that she never experienced pain as severe as the P129 daughter at any age. While P129 developed pain in her face as she got older, her mother never experienced facial pain. In parallel with the reported differences in pain severity and frequency, there were differences in medication use. P129 had a decade-long history of requiring opiates and cooling of the limbs for pain management, and these provided only partial relief. She was unable to taper/withdraw from opiates; in the past, severe withdrawal reaction occurred when attempting to withdraw from opiates under medical supervision for a clinical study. In contrast, the mother P130 reported that, throughout life, she had managed her pain with over-the-counter analgesics, and never required or used opiates.

Table 1 Summary of pain diary using NRS pain scale (0–10) over 6-week period

	Total # of attacks	Daily # of attacks	Pain attack duration (min)	Pain attack score	Overall day pain score	Pain score between attacks	Total # of awakenings	Awake duration (min)
P129	42	3.3 ± 0.1	189.8 ± 12.5	4.3 ± 0.1	3.0 ± 0.1	1.0 ± 0.2	103	40.1 ± 1.3
P130	18	0.5 ± 0.1	22.0 ± 4.2	1.2 ± 0.2	1.2 ± 0.2	0	5	19.0 ± 2.9

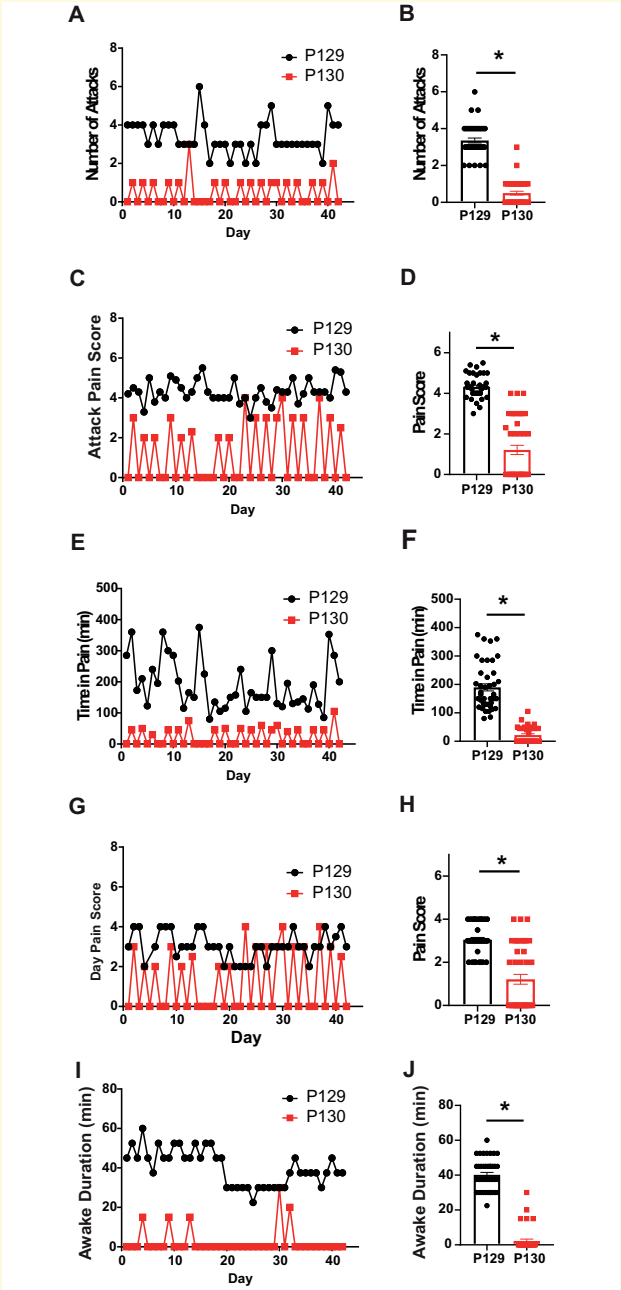

Figure 1 Pain profile based on a pain diary over a 6-week period. Pain scores were reported on a numerical rating scale (NRS) scale (0 = no pain and 10 = worst pain possible). (**A, B**) The average number of daily pain attacks for P130 was 0.5 ± 0.1 times per day, compared to 3.3 ± 0.1 pain attacks per day from P129 ($P < 0.05$). (**C, D**) Pain severity during attacks for P130 was significantly lower than that of P129, with an average pain score of 1.2 ± 0.2 (range: 2–4) versus 4.3 ± 0.1 (range: 3–6). (**E, F**) Duration of pain attacks for P130 (22.0 ± 4.2 min; range: 0–105 min) was significantly shorter than P129 (189.8 ± 12.5 min; range: 80–375 min). (**G, H**) The overall pain score during the day was significantly lower in P130 (1.2 ± 0.2) compared to P129 (3.0 ± 0.1). (**I, J**) Incidences of awakening during sleep due to pain in P129 were more prevalent and lasted 40.1 ± 1.3 min, whereas P130 had much shorter duration of 2.2 ± 1.0 min ($P < 0.05$). For all statistical analyses, an unpaired *t*-test ($P < 0.05$) was used to determine significance.

Because of these differences in their histories, both P129 and P130 were asked to complete a daily pain diary during a 6-week period, which was used to assess pain severity over time (based on NRS; 0–10) as well as the temporal profile of pain. Both subjects lived in the same geographical area, and completed their diaries at the same time. P130 described a maximum pain attack score of NRS = 4, whereas P129 reported a maximum pain attack score of NRS = 6 while on daily medications. Over the 6-week period, P130 reported fewer total number of pain attacks with 18 pain attacks compared to 42 reported by P129 (Table 1). The number of daily pain attacks for P130 was 6-fold lower, with an average of 0.5 ± 0.1 pain attacks per day compared to 3.3 ± 0.1 pain attacks per day from P129 (Fig. 1A and B; $P < 0.05$). P129 experienced ongoing pain in the feet and/or hands between attacks, often with no identifiable triggers. Pain attacks for P129 occurred spontaneously despite on-daily dosing with long-acting opiates, or were triggered by fever, heat, and exercise and occurred during sleep. P129 used cooling, elevation of feet and/or naproxen sodium in attempts to manage pain, but this often provided only partial relief. In contrast, pain attacks in P130 were milder and were triggered by exercise, and were successfully managed by elevation of feet, naproxen sodium, aspirin and/or a fan.

Pain severity during attacks for P130, as reported by the NRS pain score, was significantly lower with an average pain score of 1.2 ± 0.2 (Minimum: 2, Maximum: 4), while subject P129 reported a higher average score of 4.3 ± 0.1 (Minimum: 3, Maximum: 6; Fig. 1C and D; $P < 0.05$). Duration of pain attacks for P130 was significantly shorter than P129 with an average of 22.0 ± 4.2 min (range: 0–105 min), whereas P129 experienced average pain attack duration of 189.8 ± 12.5 min (range: 80–375 min; Fig. 1E and F; $P < 0.05$). The overall pain score during the day was significantly lower in P130 compared to P129 (Fig. 1G and H; $P < 0.05$). P130 did not experience pain between attacks (ongoing pain), whereas P129 reported ongoing pain of 2.5 ± 0.4 on the NRS pain scale. Incidences of awakening during sleep due to pain in P129 were more prevalent and lasted 40.1 ± 1.3 min, whereas P130 had much shorter duration of 2.2 ± 1.0 min (Fig. 1I and J; $P < 0.05$). These data suggest that pain attacks for P129 and P130 are both triggered by mild warmth, as is characteristic in IEM patients but with P130 reporting significantly less pain as indicated by multiple measures.

iPSC-SNs from the subject with severe pain are significantly more excitable

Genetic and functional studies of sodium channels in peripheral neurons have identified compelling evidence for the role of Nav1.7, Nav1.8 and Nav1.9 in human pain

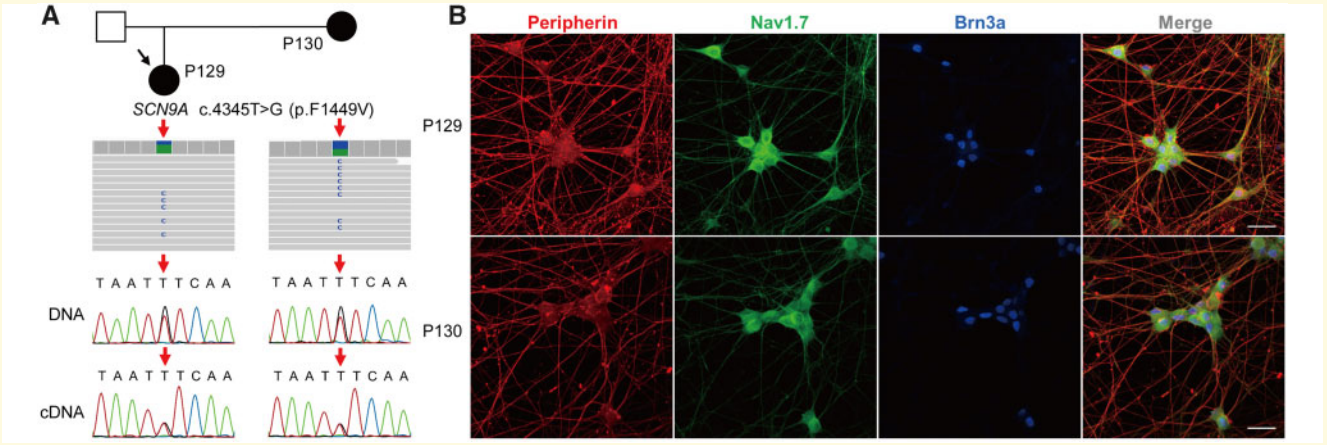

Figure 2 *SCN9A* mutation (p.F1449V) of P129 and P130, and expression of canonical peripheral markers and Nav1.7 in iPSC-SNs. (**A**) Pedigree tree and visualization of *SCN9A* mutation (c.4345T>G, p. F1449V), using Integrative Genomics Viewer (IGV) and Sanger sequencing. (**B**) All of the iPSC-SNs of P129 and P130 express peripheral neuronal marker (peripherin, red), $Na_V1.7$ channel (green), and sensory neuronal marker (brn3a, blue). Scare bar = 50 μm.

disorders.[6,25–28] Through WES, from both patients, we revalidated the c.4345T>G (p.F1449V) mutation in *SCN9A* (Fig. 2A). All coding exons and exon/intron junctions of *SCN10A and SCN11A*, encoding Nav1.8 and Nav1.9 channels, were manually confirmed to be sufficiently covered by WES for detecting heterozygous variants. We did not identify any previously reported pathogenic variants or variants considered to be potentially pathogenic based on in silico analysis in *SCN10A* or *SCN11A*.

Directed differentiation of iPSCs to sensory-like neurons yields neurons responding to noxious stimuli and exhibiting electrophysiological properties that recapitulate salient aspects of human sensory neurons.[5,18,22] We used a modified protocol described by Chambers et al.[18] to successfully differentiate patient-derived iPSCs into human sensory neurons. Mature iPSC-SNs displayed sensory-like protein expression indicated by labelling of canonical sensory neuron markers peripherin (peripheral neuronal marker for unmyelinated primary afferents), brn3a (sensory neuronal marker) and $Na_V1.7$ channel (Fig. 2B). The p. F1449V mutation of *SCN9A* was confirmed in cDNA of mature iPSC-SNs from both P129 and P130 (Fig. 2A).

Neuronal excitability is determined by a range of membrane properties in which alterations might result in inter-individual differences in sensory neuron activity. We implemented whole-cell current-clamp recordings to investigate the excitability of iPSC-SNs from subjects P129 and P130. RMP is a critical determinant of sensory neuron excitability.[29] We found that the average RMP of iPSC-SNs from subject P129 is significantly more depolarized than that of iPSC-SNs from subject P130, as can be seen in Fig. 3A ($P129 = -54.8 \pm 1$, $P130 = -57.8 \pm 1$; $t = 2.4$, $P = 0.02$, two-tailed unpaired *t*-test; n: P129 = 22, P130 = 19). Similarly, when we assessed the current threshold by applying depolarizing current steps in 5 pA increments, we found that the iPSC-SNs from P129 required significantly lower levels of stimulation to generate an AP spike ($P129 = 117 \pm 18$ pA, $P130 = 191 \pm 27$ pA, $U = 92$, $P = 0.01$; Mann–Whitney U-test; n: P129 = 20, P130 = 18, Fig. 3B). Also, neurons derived from subject P129 were more likely to fire repetitively in response to incremental 500 ms depolarizing current steps, as shown in Fig. 3C ($z = -2.3897$, $P = 0.01684$, *z*-test), which contributed to the observed significant differences in the firing rate in Fig. 3D and E ($F = 14$, $P = 0.001$; one-way repeated measures ANOVA with Bonferroni corrections; n: P129 = 22, P130 = 19). Overall, iPSC-SNs from subject 129 were more hyperexcitable than those from subject 130. The excitability patterns presented in Fig. 3 are consistent with the pain profiles reported by the two subjects.

Identification of variant Kv7.3-D755N with WES analysis

The two individuals from the same kindred in this study carry the same disease causing Nav1.7-F1449V mutation, yet they report divergent pain profiles and differences in excitability for iPSC-SNs derived from each individual. We hypothesized that a disease-modifying gene variant might contribute to the differences in excitability. Using WES of P129 and P130 with exomes captured and sequenced at an average of approximately 117-fold, and more than 98.5% of the target regions with mean coverage of 10 or higher. We compared all protein altering variants between the two patients, and a total of 320 non-overlapping variants (allele frequency < 0.01) were detected from 312 genes (Supplementary Table 1). We applied a two-step workflow to narrow down candidate genes: (i) all genes registered on the Human Pain Genes

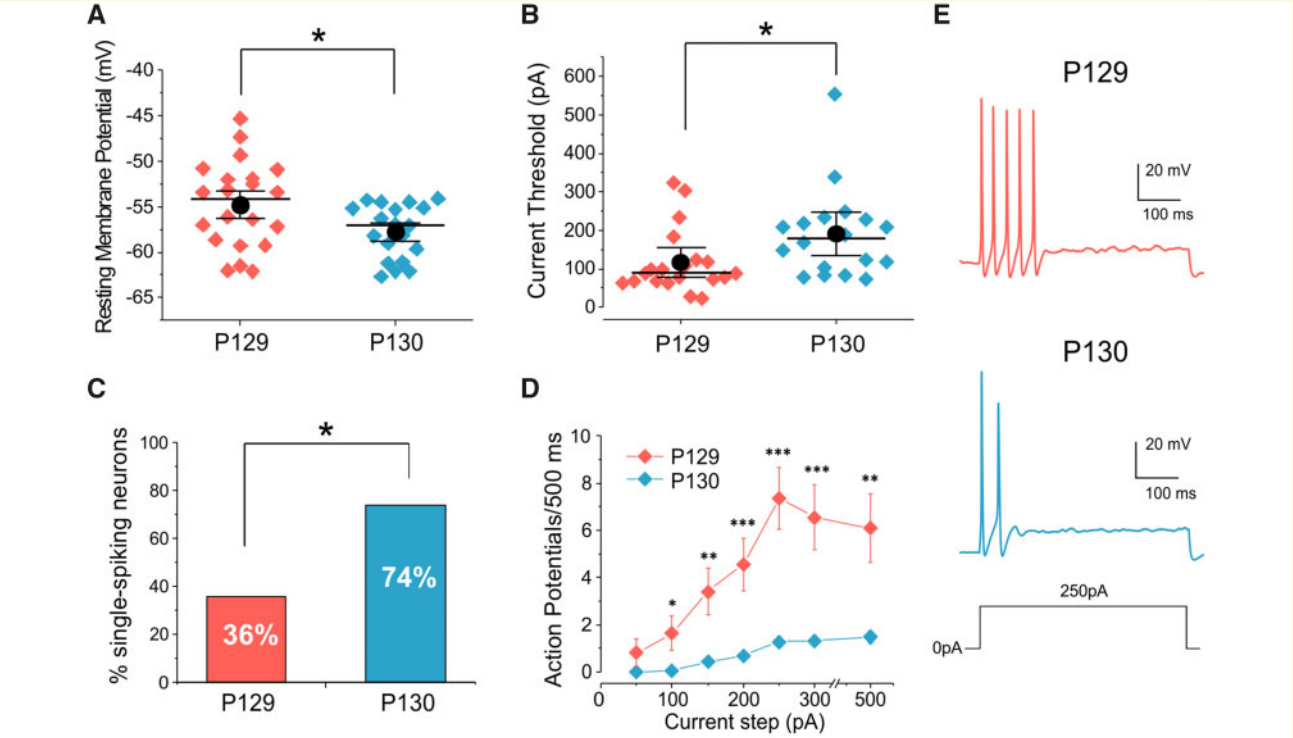

Figure 3 iPSC-SNs derived from the subject with more pain are significantly more excitable. Current-clamp recordings in sensory neurons from four independent differentiations each of iPSC from 129 and 130 subjects. (**A**) RMP values for individual iPSC-SNs from P129 and P130. Each symbol represents an individual neuron. Black circle—mean, line—median, whiskers—SE. N: P129 = 22, P130 = 19; $t = 2.4$, $P = 0.02$, two-tailed unpaired *t*-test. (**B**) Current threshold values. Each symbol represents an individual neuron. Black circle—mean, line—median, whiskers—confidence intervals. N: P129 = 20, P130 = 18; U = 92, $P = 0.01$; Mann–Whitney U-test. (**C**) Plot showing the percentage of single-spiking iPSC-SNs (P129: 12%; P130: 32%); $z = -2.3897$, $P = 0.01684$, z-test. (**D**) Input–output relationships for iPSC-SNs from P129 and P130 subjects. Data are mean ± SEM. N: P129 = 22, P130 = 19; $F = 14$, $P = 0.001$, one-way ANOVA; Bonferroni corrections for individual current steps: $^*P < 0.05$, $^{**}P < 0.001$, $^{***}P < 0.001$. (**E**) Example traces showing AP firing in iPSC-SNs from P129 and P130 in response to 500 ms 250 pA steps.

Database, which retained four genes, including *ZSCAN20*, *CACNA2D3*, *CYP3A4* and *KCNQ3*; (ii) 'Disease & Functions' analysis through IPA, which identified *KCNQ3* as the only gene linked to 'Hyperpolarization of membrane' (Fig. 4A). Within *KCNQ3*, we detected a heterozygous missense variant (frequency in gnomAD = 3.79e-4), c.2263C>T (p.D755N), from the mother patient (P130). This variant was predicted to be 'damaging' in Polyphen-2 (score = 0.721; cut-off > 0.446) and CADD_phred (score-= 24.8; cut-off > 15), and was subsequently confirmed in the genome of the subject using Sanger sequencing (Fig. 4B). This Kv7.3-D755N variant was also validated from cDNA of mature iPSC-SNs of P130 (Fig. 4B), and alters a highly conserved residue in the C-terminal intracellular domain of the channel (Fig. 4C and D).

Voltage-clamp characterization of Kv7.3-D755N

Kv7.3 is known to contribute to the M-current and, together with Kv7.2 [encoded by *KCNQ2* (MIM: 602235)], modulate the excitability of DRG neurons.[30,31] To investigate whether the current produced by Kv7.3-D755N contributes to reduced neuronal excitability of P130 iPSC-SN, we examined the gating properties of the Kv7.3-D755N variant by voltage-clamp of transiently transfected HEK293 cells. HEK cells express very small outward currents which thereby allowing better biophysical characterization of heterologously expressed Kv7 channels compared to heterologous expression in sensory neurons which already express endogenous outward currents. Native M-current is composed of a heteromeric complex of Kv7.2 and Kv7.3 α-subunits, and attempts to record from homomeric Kv7.3 transiently transfected into HEK293 cells have been previously shown to produce very small currents,[32,33] therefore, currents produced by the co-transfection of Kv7.2 and Kv7.3 constructs were analysed. The co-expression of Kv7.2-WT and Kv7.3-WT elicits slowly activating outward currents in response to depolarizing voltage pulses as shown in Fig. 5A. The current–voltage relationship curve was constructed by plotting the peak outward current versus the stimulation potential. (Fig. 5B) The G–V curve is determined by utilizing the peak 'tail current' during the −120 mV pulse

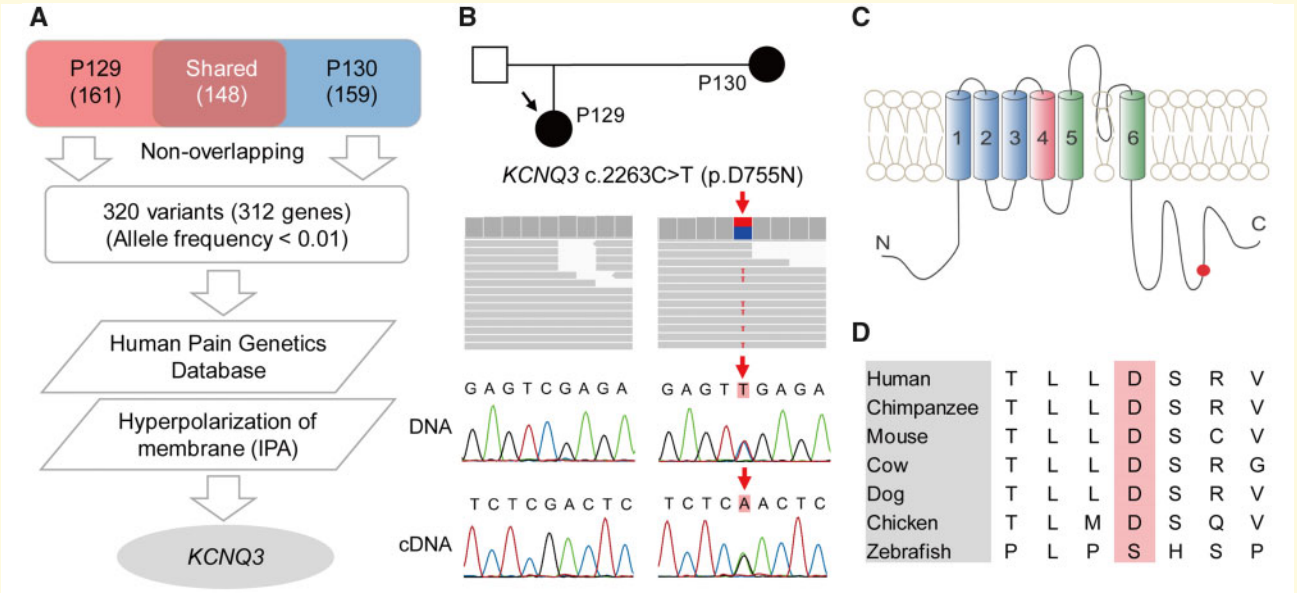

Figure 4 Identification of p. D755N in *KCNQ3*. (**A**) WES variant analysis workflow between P129 and P130. (**B**) Pedigree tree and visualization of *KCNQ3* variant (c.2263C>T, p. D755N), using Integrative Genomics Viewer and Sanger sequencing. (**C**) Schematic diagram of Kv7.3 showing the location of p. D755N. (**D**) D755 residue is highly conserved among various species.

and whose value will be proportional to the conductance achieved at the end of the preceding stimulation pulse (Fig. 5C). To determine if the gating properties vary with time after initiating whole-cell configuration, the activation stimulation protocol was repeated at various times and the resulting current–voltage relationship curves are plotted as shown (Fig. 5D).

The primary change with time after initiating whole-cell configuration is a partial reduction of conductance. For these cells, most of the reduction of conductance occurred during the first 10 min and seemed to reach a steady-state level by 20 min. For comparison, the currents elicited by transfecting HEK293 cells with Kv7.2-WT and Kv7.3-D755N were examined. The currents elicited by depolarizing pulses are similar to those elicited when using the Kv7.3-WT construct (Fig. 5E) and also demonstrate reduction of conductance over time (Fig. 5F). For cells co-expressing Kv7.2-WT and Kv7.3-WT (WT M-current), the reduction of current density was significant after 10 min and averaged 42% reduction ($P < 0.001$; $n = 12$ by mixed effect ANOVA). Similarly, cells expressing Kv7.2-WT and Kv7.3-D755N (variant M-current) exhibited reduction, but to an apparent lesser extent, which averaged 20% after ten minutes ($P = 0.002$; $n = 12$ by mixed effect ANOVA). Although the average variant M-current started slightly larger than WT M-current, the average variant M-current was significantly larger than WT M-current after ten minutes (Fig. 5G; $P = 0.02$; $n = 12$ by mixed effect ANOVA).

The excitability of iPSC-SNs is modulated by Kv7.3-D755N M-current levels

Based on the voltage-clamp results from Kv7 channels heterologously expressed in HEK293 cells, M-current of iPSC-SNs containing the Kv7.3-D755N variant should be significantly more resistant to reduction in current compared to cells expressing the Kv7.3-WT channel. We have shown that iPSC-SNs from a related pair of IEM patients (both carrying the disease-related mutation of Nav1.7-F1449V) exhibited differences in excitability where the patient expressing the Kv7.3-D755N variant was less excitable compared to the patient carrying the Kv7.3-WT channel. The iPSC sensory neurons express multiple outward currents of which M-currents (comprised of heteromultimers of Kv7.2 and Kv7.3 proteins) are able to be measured cleanly in only a narrow range of membrane potentials. Using the voltage protocol as utilized in Mis et al.,[5] there was no significant difference in the M-current measured shortly after achieving whole-cell configuration from the holding potential of −20 mV between iPSC sensory neurons derived from patient 129 (20.4 ± 5.9 pA $n = 9$) or 130 (24.9 ± 7.4 pA, $n = 7$). Assuming the reduction of conductance seen in HEK cells also occurs in the iPSC sensory neurons, the modulatory effect of the Kv7.3-D755N variant on the excitability of iPSC-derived sensory neurons, was assessed by dynamic-clamp which allowed us to evaluate the impact of

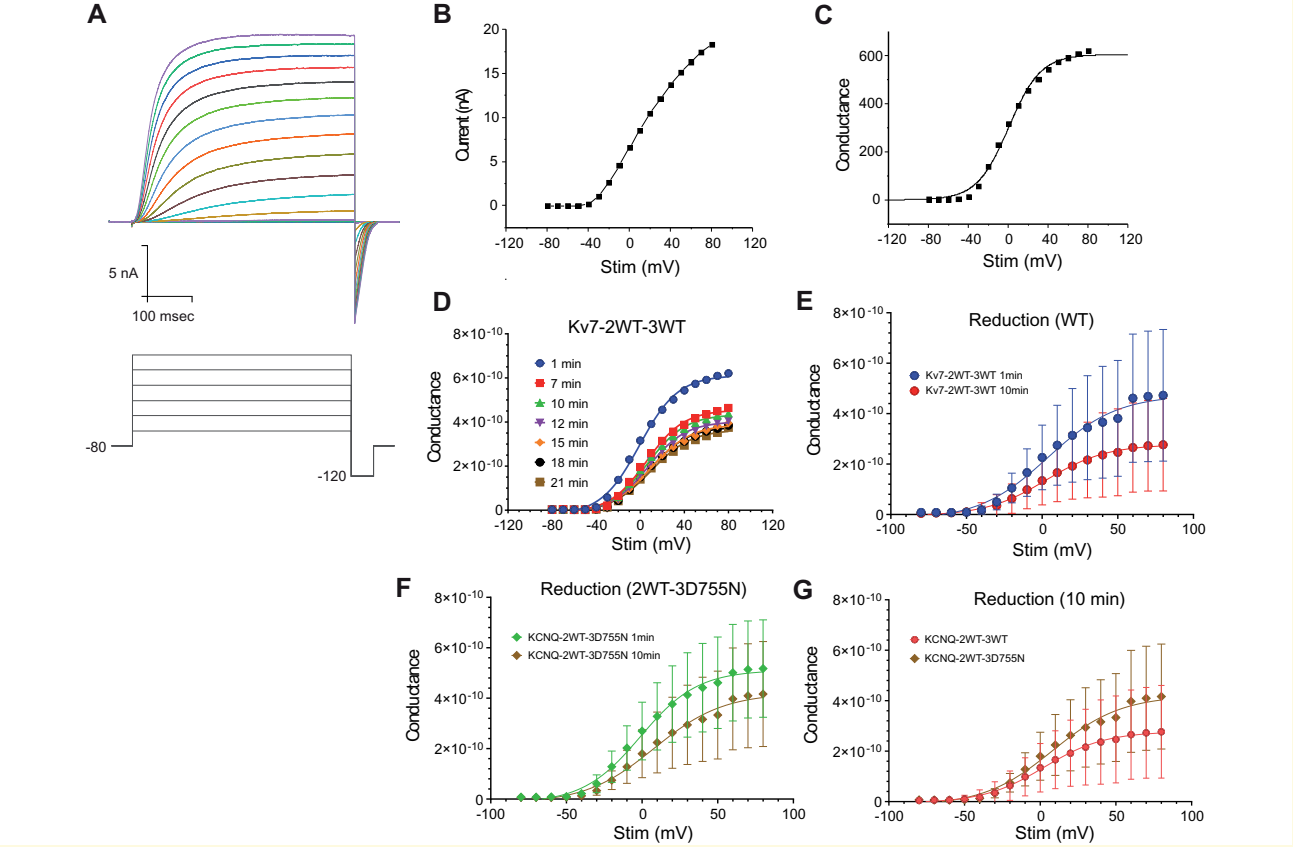

Figure 5 Kv7.3-D755N is resistant to time-dependent reduction. (**A**) Example traces of currents elicited by a series of voltage depolarizations as illustrated by the schematic below the traces. (**B**) The maximal outward current is plotted as a function of the stimulation potential to generate the I–V curve. (**C**) The G–V curve was determined by measuring the instantaneous inward current in response to the repolarizing pulse to −120 mV and then normalized for cell size by dividing by cell capacitance. (**D**) The conductance from this cell reduced with time over 20 min determined by repeating the I–V protocol at the times indicated by the legend. (**E**) The averaged conductance just after initiating whole-cell and after waiting 10 min for cells expressing Kv7.2-WT/Kv7.3-WT. The reduction of conductance was significantly reduced by 43% ($P < 0.001$, mixed effect ANOVA, $n = 12$). (**F**) The averaged conductance just after initiating whole-cell and after waiting 10 min for cells expressing Kv7.2-WT/Kv7.3-D755N. The reduction of conductance was significantly reduced by 20% ($P < 0.001$, mixed effect ANOVA, $n = 12$). (**G**) The averaged conductance of the Kv7.2-WT/Kv7.3-WT washed out to a larger extent over ten minutes compared to Kv7.2-WT/Kv7.3-D755N. The WT conductance was significantly reduced by 33% compared to D755N variant conductance ($P = 0.02$, mixed effect ANOVA, $n = 12$).

impaired reduction of conductance of a channel variant such as Kv7.3-D755N by injecting controlled amounts of a model of M-current into a cell. Neuronal excitability was determined by a range of membrane properties, alterations in which might result in inter-individual differences in sensory neuron activity. We implemented whole-cell dynamic-clamp to investigate the changes of excitability of iPSC-SNs from subjects P129 (Kv7.3-WT, severe pain) and P130 (Kv7.3-D755N, mild pain) when M-current density is varied. Each cell could be evaluated before-and-after calibrated electronic alteration of the M-current.

The effect of restoring M-current on iPSC-SNs derived from P129 (who carries WT Kv7.3 alleles) shows a dampening of excitability as additional M-current is introduced (Fig. 6). Incremental current injections with dynamic-clamp OFF (Fig. 6A) and the same cell with dynamic-clamp ON (Fig. 6B) show repetitive firing of APs in the family of traces from patient-derived iPSC-SNs. The injected currents (bottom: Fig. 6A and B) are the net current of the current stimulus as well as the calculated amount of the model M current that responds to the varying membrane potential of the neuron. Quantifying of the spike activity elicited as a function of stimulus showed, as expected, an overall decrease in excitability when additional M-current is added back using a dynamic-clamp model of native M-current (Fig. 6C). On average, supplementing the average amount of M-current that washes out over ten minutes back to iPSC-SNs expressing the wild-type of M-current (P129) resulted in a significant reduction of excitability (Fig. 6D, $P < 0.001$; $n = 12$ by repeated measures ANOVA).

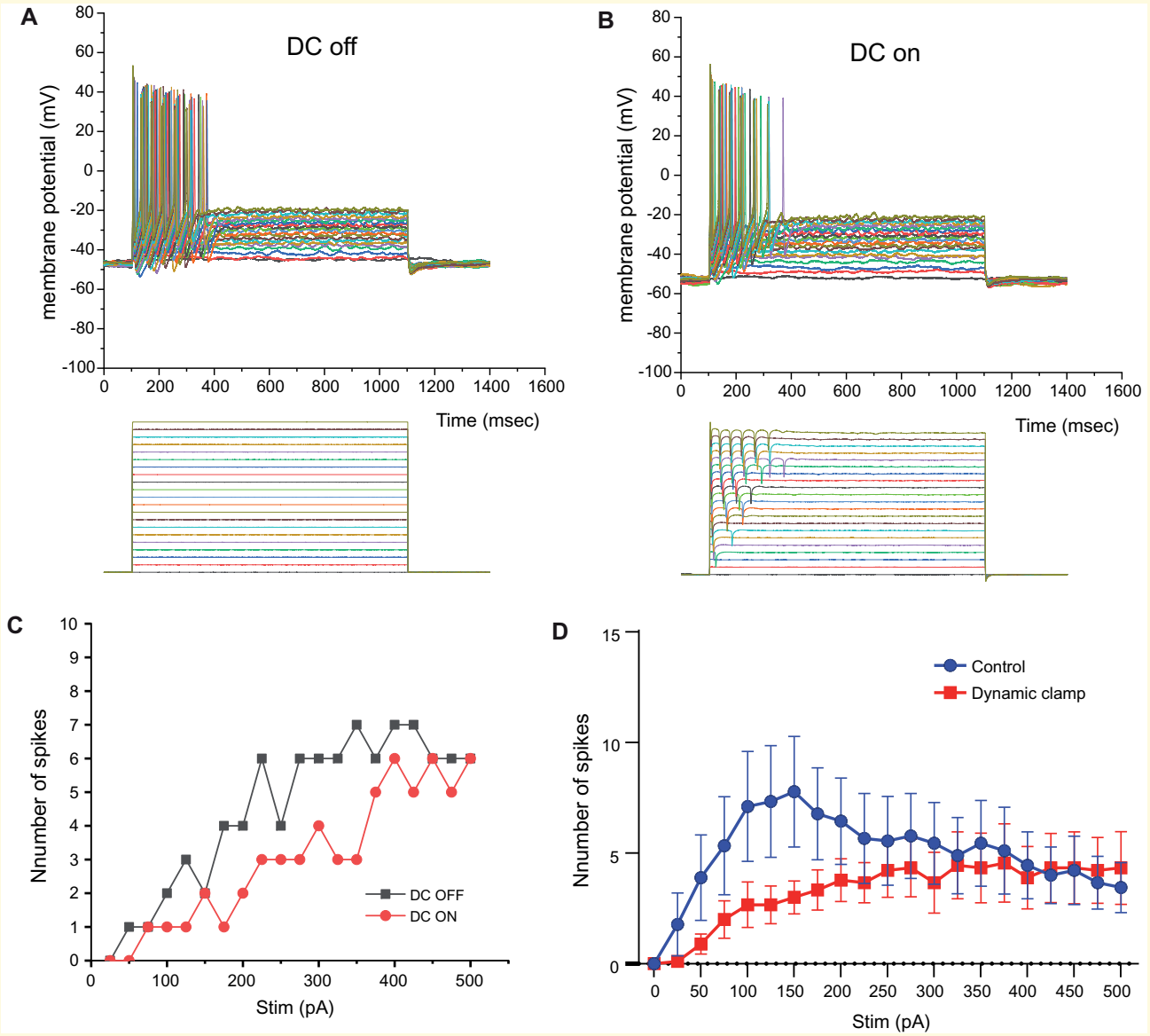

Figure 6 Dynamic clamp addition of M-current modulates excitability. (**A**) Example traces recorded from patient-derived iPSC-sensory neuron in current-clamp mode with dynamic-clamp circuit turned OFF. The AP activity of selected stimuli was elicited by depolarizing current injections as illustrated by the inset below the figure and of the values listed by the legend. The scale bar axes are shared with the mV value corresponding to the traces and the pA value corresponding to the stimuli. (**B**) Example traces recorded from the same cell shown in panel A in response to the same depolarizing current stimuli with the addition of additional M-current by turning the dynamic-clamp circuit ON. The modelled additional current is clearly visible in the injected current traces shown in the inset below. (**C**) The number of spikes elicited is plotted as a function of the injected current stimulus from the entire dataset collected. (**D**) The averaged effect of adding only 1nS of M-current (~50 pS/pF) by dynamic-clamp recording from patient-derived iPSC-sensory neurons (clone-129 who expresses KCNQ-WT currents) was a significant reduction of the firing-frequency response ($P < 0.01$, $n = 9$ by repeated measures ANOVA).

Discussion

In this study, we capitalized on the availability of a well-phenotyped daughter–mother pair with painful IEM due to the same Nav1.7-F1449V gain-of-function mutation, in which we documented distinct differences in salient pain features, and validated the 'pain-resilience-in-a-dish' model that we have recently developed.[5] Despite carrying the same gain-of-function Nav1.7 mutation, we show significant differences among the pain features quantified here between the mother and her daughter, suggesting a contribution of possible private modulatory gene variants that introduce inter-individual differences into the pain experience. While we cannot entirely rule out environmental contributions to the pain profiles in these two subjects, they resided in the same geographical area and

were studied at the same time, suggesting that environmental differences were not substantial contributors to their different pain profiles. We demonstrated that differences in excitability of patient-specific iPSC-SN from these two subjects paralleled differences in their pain phenotype, pointing to a pain resilience factor in peripheral sensory neurons. WES and *in silico* analyses identified a variant in Kv7.3 in the resilient mother and functional testing provided evidence for a role of this variant in regulating excitability of iPSC-SNs further supporting a peripheral component to pain resilience, and providing a demonstration of the utility of our 'pain-resilience-in-a-dish' iPSC-derived model as a tool for detection of pain-modifying factors. Our results point to a variant in *KCNQ3*, acting within peripheral sensory neurons, as a modulator of the pain profile in the pain-resilient subject.

To date, 25 gain-of-function mutations of Nav1.7 have been described as causative in IEM, all of which produce hyperpolarizing shift in channel activation.[6,34] Deep phenotyping has revealed significant differences in pain symptoms within family members carrying the same mutation.[16,35] Although inter-individual differences in pain even among closely related individuals are well documented, they are not well understood. The p. F1449V mutation reduces current threshold for APs and causes a higher firing frequency of nociceptors.[10] Until recently, functional studies of p. F1449V and other Nav1.7 IEM mutations relied on the expression of the mutant channels in rodent DRG neurons to assess the effect of the mutations at the neuronal level. However, these studies cannot identify molecular mechanisms that underlie inter-individual variability in pain that have been reported in patients carrying Nav1.7 mutations.[16,35]

Directed differentiation of iPSCs that yield sensory-like neurons which recapitulate salient aspects of human sensory neurons provides an opportunity to correlate excitability of these iPSC-SNs with pain phenotypes. Starting with a pair of well-phenotyped mother/son subjects with IEM and the Nav1.7-S241T mutation, we have recently shown that the relative sensitivity to pain is paralleled by different excitability properties of patient-specific iPSC-SN *in vitro*, suggesting that at least in some cases, mechanisms operating in peripheral sensory neurons may contribute to inter-individual differences in pain.[5,18,22] Our current study of a mother/daughter pair carrying a different Nav1.7 mutation, p. F1449V, with quantifiable differences in pain, confirmed that iPSC-SNs of the pain-resilient patient are less excitable than those of the more severely affected patient. Using WES and dynamic clamp, we have now identified specific gene variants in two members of the Kv7 family, in the Kv7.2 and Kv7.3 (current study), that modulate excitability of the iPSC-SNs, providing a mechanistic explanation for inter-individual differences in pain in these pairs of patients. Together, these two studies validate this powerful platform for studying 'pain-resilience-in-a-dish' for the discovery of novel gene variants that modify pain, and suggest that this approach may be applicable to other kindreds with similar phenotype–genotype characteristics.

WES identified the p. D755N variant in Kv7.3 among 320 of rare non-overlapping variants in P129 and P130. Kv7.2 and Kv7.3 channels (encoded by *KCNQ2 and KCNQ3*, respectively) share a similar 6 transmembrane structure as other voltage-gated potassium channels,[36,37] and assemble into homotetrameric, or heterotetrameric channels which generate the subthreshold, non-inactivating M-current.[38] They have been found at multiple sites within the pain transmission pathway, including nociceptors, spinal cord and cerebral cortex circuits.[39] Kv7.2/Kv7.3 channels are preferentially enriched at the axon initial segments, the origin site of APs, as well as nodes of Ranvier of myelinated axons and at nerve terminals in myelinated and unmyelinated fibres.[40–42] These channels can open at RMPs and are responsible for the generation of slowly-inactivating potassium M-current, which is a critical modulator of membrane potential and can function as a brake on the excitability of central and peripheral neurons to impede repetitive neuronal firing.[43,44]

Heteromeric Kv7.2/Kv7.3 channel, rather than homomeric Kv7.2 or Kv7.3 channel, produce robust M-current.[32,33] In this study, Kv7.2/Kv7.3 co-transfected HEK293 cells produced the expected M-current, and the current–voltage relationship showed that co-expression of Kv7.2-WT/Kv7.3-D755N channels yielded similar current densities as that of Kv7.2-WT/Kv7.3-WT. However, as the recording period increased, the Kv7.2-WT/Kv7.3-D755N current density became statistically bigger than that of WT channels because of less time-dependent reduction in the current. The p. D755N substitution is located in the C-terminal cytoplasmic region of the protein and is the region proposed to have regulatory interactions with intracellular signalling pathways.[45] We utilized a pipette solution designed to support stability of metabolically regulated ion channels, especially avoiding the use of fluoride which is known to activate G-proteins, resulting in small KCNQ current.[46] The significantly slowed or impaired time-dependent down-regulation could be considered a gain-of-function attribute for this variant since this phenotype would be predicted to reduce the excitability of sensory neurons. It is also possible that painful episodes activate inflammatory signalling that includes downregulation of M-current downstream of G-protein activation which might be lessened in the mother if the Kv7.3-D755N variant is differentially resistant to downregulation. Indeed, supplementing a modest amount of M-current to iPSC-SNs using dynamic-clamp significantly reduced the excitability of these neurons. This finding is consistent with the difference in pain phenotype of the two subjects, with the mother patient (P130) with Kv7.3-D755N experiencing relatively milder pain compared to the daughter (P129) with severe pain.

Consistent with their regulation of neuron firing properties, loss-of-function mutations of both Kv7.2 and

Kv7.3 have been implicated in a hyperexcitability-related disorder, benign familial neonatal seizures (MIM: 121200).[47] The mechanisms underlying loss-of-function mutations of *Kv7.3* include haploinsufficiency, gating alterations and dominant-negative effect.[41] Beyond benign familial neonatal seizures, mutations of *KCNQ3* have also been associated with other clinical entities, including intellectual disability, neurodevelopmental disorders and autism.[48,49] Gain-of-function features, increased current density and hyperpolarized voltage-dependence of activation of multiple variants in Kv7.3 have been found in patients with autism and developmental disabilities.[49] Whether these subjects with gain-of-function mutations in Kv7.2/Kv7.3 experience less pain is not well understood. An association between reduction of Kv7.2/Kv7.3 channel activity and neuropathic pain has also been proposed.[50] Opening M-channels, such as Kv7.2 and Kv7.3, attenuates nociceptive behaviours in various animal models of pain, including inflammatory, neuropathic and cancer pain.[30,31] The gain-of-function mutations in Kv7.2 and Kv7.3 that we have identified in the two pairs of IEM patients in our studies can have significant effect on neuronal excitability and are associated with the pain resilience phenotype in the carriers of these mutations, providing a link to human pain.

Some of the compounds that have been reported to modulate M-current act as strong positive allosteric modulators.[51] Retigabine, for example, thought to bind to the membrane-spanning regions of Kv7.2 or Kv7.3 and strongly alter the energetics of voltage-dependent gating,[52,53] shows a concentration-dependent leftward shift of activation voltage-dependence that can exceed 40 mV.[54] Mis (2019) study reported a change in the voltage-dependence of activation for Kv7.2-T730A that was significantly different at membrane potentials falling between the RMP and AP threshold, whereas this study showed increased current density for M-currents containing Kv7.3-D755N channels. Although both of these changes were of modest magnitude, they caused a significant effect on the excitability of the iPSC-SNs. Our results suggest that pain resilience may be achievable with concentrations of Kv7 activators that are well below the EC50 values documented in drug discovery studies or with new compounds that do not shift properties into the range associated with pathophysiological conditions.

This study builds upon our unique database of kindreds and demonstrates the role of M-currents in modulating the pain experience for individuals with IEM, a human genetic model of neuropathic pain.[5] Our patient-specific iPSC-SNs not only exhibit hyperexcitability associated with pain, but also display individual-specific differences that parallel clinical phenotype, providing validation of the 'pain-resilience-in-a-dish' model using patient-specific iPSC-SNs. From the mother patient with mild pain, we identified the Kv7.3-D755N variant which is predicted to contribute to resilience to pain and showed that it reduces excitability in iPSC-SNs. We would stress that our results do not rule out other contributors to pain resilience in P130. It is, for example, possible that our analysis may have missed a contribution from genes of unknown function yet to be linked to pain pathways, non-coding RNAs, or genomic copy number variations. Moreover, our analysis focussed on peripheral sensory neurons, and did not assess the effects of genes expressed at higher levels (e.g. spinal, supra-spinal) in the CNS where additional mechanisms could have further modulated the pain profile. Nonetheless, our results are notable in pinpointing *KCNQ3* and in showing that it contributes to pain resilience at least in part via an action within peripheral sensory neurons. Our observations indicate that iPSC-SNs, from two subjects in the same family, both carrying the same gain-of-function Nav1.7 mutation but with different pain profiles, display different degrees of hyperexcitability that parallel their pain profile. WES and electrophysiological analysis demonstrated that a *KCNQ3* variant, a gain-of-function mutation of Kv7.3, contributes to pain resilience in the subject with less pain, via an action in peripheral sensory neurons. Taken together, the current results support the conclusion that variants of the KCNQ family can act at a peripheral level to modulate sensory neuron excitability and contribute to pain resilience.

Supplementary material

Supplementary material is available at *Brain Communications* online.

Acknowledgements

We thank patients in this study for their participation. We also thank Daniel Sosniak for excellent technical support.

Funding

This work was supported by Center Grant B9253-C from the U.S. Department of Veterans Affairs Rehabilitation Research and Development Service, by a grant from The Erythromelalgia Association, and by the Regenerative Medicine Research Fund of CT Innovations. The Center for Neuroscience and Regeneration Research is a Collaboration of the Paralyzed Veterans of America with Yale University.

Competing interests

The authors report no competing interests.

References

1. Lotsch J, Doehring A, Mogil JS, Arndt T, Geisslinger G, Ultsch A. Functional genomics of pain in analgesic drug development and therapy. Pharmacol Ther. 2013;139(1):60–70.
2. Dib-Hajj SD, Waxman SG. Translational pain research: Lessons from genetics and genomics. Sci Transl Med. 2014;6(249):249sr4.
3. Zorina-Lichtenwalter K, Meloto CB, Khoury S, Diatchenko L. Genetic predictors of human chronic pain conditions. Neuroscience. 2016;338:36–62.
4. Mogil JS. Pain genetics: Past, present and future. Trends Genet. 2012;28(6):258–266.
5. Mis MA, Yang Y, Tanaka BS, et al. Resilience to pain: A peripheral component identified using induced pluripotent stem cells and dynamic clamp. J Neurosci. 2019;39(3):382–392.
6. Bennett DL, Clark AJ, Huang J, Waxman SG, Dib-Hajj SD. The role of voltage-gated sodium channels in pain signaling. Physiol Rev. 2019;99(2):1079–1151.
7. Dib-Hajj SD, Waxman SG. Sodium channels in human pain disorders: Genetics and pharmacogenomics. Annu Rev Neurosci. 2019; 42:87–106.
8. Drenth JP, Waxman SG. Mutations in sodium-channel gene SCN9A cause a spectrum of human genetic pain disorders. J Clin Invest. 2007;117(12):3603–3609.
9. Cummins TR, Dib-Hajj SD, Waxman SG. Electrophysiological properties of mutant Nav1.7 sodium channels in a painful inherited neuropathy. J Neurosci. 2004;24(38):8232–8236.
10. Dib-Hajj SD, Rush AM, Cummins TR, et al. Gain-of-function mutation in Nav1.7 in familial erythromelalgia induces bursting of sensory neurons. Brain. 2005;128(Pt 8):1847–1854.
11. Yang Y, Wang Y, Li S, et al. Mutations in SCN9A, encoding a sodium channel alpha subunit, in patients with primary erythermalgia. J Med Genet. 2004;41(3):171–174.
12. Alschuler KN, Kratz AL, Ehde DM. Resilience and vulnerability in individuals with chronic pain and physical disability. Rehabil Psychol. 2016;61(1):7–18.
13. Lorsch ZS, Hamilton PJ, Ramakrishnan A, et al. Stress resilience is promoted by a Zfp189-driven transcriptional network in prefrontal cortex. Nat Neurosci. 2019;22(9):1413–1423.
14. Maul S, Giegling I, Fabbri C, Corponi F, Serretti A, Rujescu D. Genetics of resilience: Implications from genome-wide association studies and candidate genes of the stress response system in posttraumatic stress disorder and depression. Am J Med Genet B Neuropsychiatr Genet. 2020;183(2):77–94.
15. McIntosh AM, Sullivan PF, Lewis CM. Uncovering the genetic architecture of major depression. Neuron. 2019;102 (1):91–103.
16. Geha P, Yang Y, Estacion M, et al. Pharmacotherapy for pain in a family with inherited erythromelalgia guided by genomic analysis and functional profiling. JAMA Neurol. 2016;73(6): 659–667.
17. Cao L, McDonnell A, Nitzsche A, et al. Pharmacological reversal of a pain phenotype in iPSC-derived sensory neurons and patients with inherited erythromelalgia. Sci Transl Med. 2016;8(335): 335ra56.
18. Chambers SM, Qi Y, Mica Y, et al. Combined small-molecule inhibition accelerates developmental timing and converts human pluripotent stem cells into nociceptors. Nat Biotechnol. 2012; 30(7):715–720.
19. Di Stefano G, Yuan JH, Cruccu G, Waxman SG, Dib-Hajj SD, Truini A. Familial trigeminal neuralgia – A systematic clinical study with a genomic screen of the neuronal electrogenisome. Cephalalgia. 2020;40(8):767–777.
20. Yuan JH, Schulman BR, Effraim PR, Sulayman DH, Jacobs DS, Waxman SG. Genomic analysis of 21 patients with corneal neuralgia after refractive surgery. Pain Rep. 2020;5(4):e826.
21. Liu X, Wu C, Li C, Boerwinkle E. dbNSFP v3.0: A one-stop database of functional predictions and annotations for human nonsynonymous and splice-site SNVs. Hum Mutat. 2016;37(3): 235–241.
22. Young GT, Gutteridge A, Fox H, et al. Characterizing human stem cell-derived sensory neurons at the single-cell level reveals their ion channel expression and utility in pain research. Mol Ther. 2014;22(8):1530–1543.
23. Labau JIR, Estacion M, Tanaka BS, et al. Differential effect of lacosamide on Nav1.7 variants from responsive and non-responsive patients with small fibre neuropathy. Brain. 2020;143(3):771–782.
24. Yang Y, Huang J, Mis MA, et al. Nav1.7-A1632G mutation from a family with inherited erythromelalgia: Enhanced firing of dorsal root ganglia neurons evoked by thermal stimuli. J Neurosci. 2016; 36(28):7511–7522.
25. Bennett DL, Woods CG. Painful and painless channelopathies. Lancet Neurol. 2014;13(6):587–599.
26. Dib-Hajj SD, Black JA, Waxman SG. NaV1.9: A sodium channel linked to human pain. Nat Rev Neurosci. 2015;16(9):511–519.
27. Dib-Hajj SD, Yang Y, Black JA, Waxman SG. The Na(V)1.7 sodium channel: From molecule to man. Nat Rev Neurosci. 2013; 14(1):49–62.
28. Han C, Huang J, Waxman SG. Sodium channel Nav1.8: Emerging links to human disease. Neurology. 2016;86(5):473–483.
29. Huang J, Mis MA, Tanaka B, et al. Atypical changes in DRG neuron excitability and complex pain phenotype associated with a Nav1.7 mutation that massively hyperpolarizes activation. Sci Rep. 2018;8(1):1811.
30. Du X, Gao H, Jaffe D, Zhang H, Gamper N. M-type K(+) channels in peripheral nociceptive pathways. Br J Pharmacol. 2018; 175(12):2158–2172.
31. Wu Z, Li L, Xie F, et al. Activation of KCNQ channels suppresses spontaneous activity in dorsal root ganglion neurons and reduces chronic pain after spinal cord injury. J Neurotrauma. 2017;34(6): 1260–1270.
32. Schwake M, Pusch M, Kharkovets T, Jentsch TJ. Surface expression and single channel properties of KCNQ2/KCNQ3, M-type K+ channels involved in epilepsy. J Biol Chem. 2000;275(18):13343–13348.
33. Selyanko AA, Hadley JK, Brown DA. Properties of single M-type KCNQ2/KCNQ3 potassium channels expressed in mammalian cells. J Physiol. 2001;534(Pt 1):15–24.
34. Dib-Hajj SD, Cummins TR, Black JA, Waxman SG. Sodium channels in normal and pathological pain. Annu Rev Neurosci. 2010; 33:325–347.
35. McDonnell A, Schulman B, Ali Z, et al. Inherited erythromelalgia due to mutations in SCN9A: Natural history, clinical phenotype and somatosensory profile. Brain. 2016;139(Pt 4):1052–1065.
36. Long SB, Campbell EB, Mackinnon R. Crystal structure of a mammalian voltage-dependent Shaker family K+ channel. Science. 2005;309(5736):897–903.
37. Sun J, MacKinnon R. Cryo-EM structure of a KCNQ1/CaM complex reveals insights into congenital long QT syndrome. Cell. 2017;169(6):1042–1050.e1049.
38. Brown DA, Passmore GM. Neural KCNQ (Kv7) channels. Br J Pharmacol. 2009;156(8):1185–1195.
39. Hayashi H, Iwata M, Tsuchimori N, Matsumoto T. Activation of peripheral KCNQ channels attenuates inflammatory pain. Mol Pain. 2014;10:15.
40. Devaux JJ, Kleopa KA, Cooper EC, Scherer SS. KCNQ2 is a nodal K+ channel. J Neurosci. 2004;24(5):1236–1244.
41. Maljevic S, Wuttke TV, Lerche H. Nervous system KV7 disorders: Breakdown of a subthreshold brake. J Physiol. 2008;586(7): 1791–1801.
42. Vervaeke K, Gu N, Agdestein C, Hu H, Storm JF. Kv7/KCNQ/M-channels in rat glutamatergic hippocampal axons and their role in regulation of excitability and transmitter release. J Physiol. 2006; 576(Pt 1):235–256.
43. Brown DA, Adams PR. Muscarinic suppression of a novel voltage-sensitive K+ current in a vertebrate neurone. Nature. 1980; 283(5748):673–676.

44. Robbins J. KCNQ potassium channels: Physiology, pathophysiology, and pharmacology. Pharmacol Ther. 2001;90(1):1–19.
45. Haitin Y, Attali B. The C-terminus of Kv7 channels: A multifunctional module. J Physiol. 2008;586(7):1803–1810.
46. Suh BC, Horowitz LF, Hirdes W, Mackie K, Hille B. Regulation of KCNQ2/KCNQ3 current by G protein cycling: The kinetics of receptor-mediated signaling by Gq. J Gen Physiol. 2004;123(6):663–683.
47. Charlier C, Singh NA, Ryan SG, et al. A pore mutation in a novel KQT-like potassium channel gene in an idiopathic epilepsy family. Nat Genet. 1998;18(1):53–55.
48. Rauch A, Wieczorek D, Graf E, et al. Range of genetic mutations associated with severe non-syndromic sporadic intellectual disability: An exome sequencing study. Lancet. 2012;380(9854):1674–1682.
49. Sands TT, Miceli F, Lesca G, et al. Autism and developmental disability caused by KCNQ3 gain-of-function variants. Ann Neurol. 2019;86(2):181–192.
50. Munro G, Dalby-Brown W. Kv7 (KCNQ) channel modulators and neuropathic pain. J Med Chem. 2007;50(11):2576–2582.
51. Wang AW, Yau MC, Wang CK, et al. Four drug-sensitive subunits are required for maximal effect of a voltage sensor-targeted KCNQ opener. J Gen Physiol. 2018;150(10):1432–1443.
52. Padilla K, Wickenden AD, Gerlach AC, McCormack K. The KCNQ2/3 selective channel opener ICA-27243 binds to a novel voltage-sensor domain site. Neurosci Lett. 2009;465(2):138–142.
53. Syeda R, Santos JS, Montal M. The sensorless pore module of voltage-gated K+ channel family 7 embodies the target site for the anticonvulsant retigabine. J Biol Chem. 2016;291(6):2931–2937.
54. Yau MC, Kim RY, Wang CK, et al. One drug-sensitive subunit is sufficient for a near-maximal retigabine effect in KCNQ channels. J Gen Physiol. 2018;150(10):1421–1431.